ADVANCES IN ATMOSPHERIC SCIENCES, VOL. 24, NO. 2, 2007, 1–18

Probability Distribution Function of a Forced Passive Tracer in the Lower Stratosphere

HU Yongyun* (胡永云)

Department of Atmospheric Sciences, School of Physics, Peking University, Beijing 100871

(Received 20 February 2006; revised 7 July 2006)

ABSTRACT

The probability distribution function (PDF) of a passive tracer, forced by a "mean gradient", is studied. First, we take two theoretical approaches, the Lagrangian and the conditional closure formalisms, to study the PDFs of such an externally forced passive tracer. Then, we carry out numerical simulations for an idealized random flow on a sphere and for European Center for Medium-Range Weather Forecasts (ECMWF) stratospheric winds to test whether the mean-gradient model can be applied to studying stratospheric tracer mixing in midlatitude surf zones, in which a weak and poleward zonal-mean gradient is maintained by tracer leakage through polar and tropical mixing barriers, and whether the PDFs of tracer fluctuations in midlatitudes are consistent with the theoretical predictions. The numerical simulations show that when diffusive dissipation is balanced by the mean-gradient forcing, the PDF in the random flow and the Southern-Hemisphere PDFs in ECMWF winds show time-invariant exponential tails, consistent with theoretical predictions. In the Northern Hemisphere, the PDFs exhibit non-Gaussian tails. However, the PDF tails are not consistent with theoretical expectations. The long-term behavior of the PDF tails of the forced tracer is compared to that of a decaying tracer. It is found that the PDF tails of the decaying tracer are time-dependent, and evolve toward flatter than exponential.

Key words: chaotic mixing, probability distribution function, stratosphere, turbulence, passive tracer

DOI:

1. Introduction

Tracer mixing is one of the important problems in atmospheric sciences, and one of the central problems in tracer mixing is to charaterize small-scale fluctuations of tracer concentrations. In the past decade, probability distribution functions (PDFs) of tracer fluctuations have been used extensively in turbulence research, such as laboratory experiments (Castaing et al., 1989; Jayesh and Warhaft, 1992; Gollub et al., 1991; Warhaft, 2000) and theoretical works (Sinai and Yakhot, 1989; Pumir, 1994; Majda, 1993; Shraiman and Siggia, 1994; Chertkov et al., 1995; Sreenivasan and Antonia, 1997; Balkovsky and Fouxon, 1999; Majda and Kramer, 1999; Pierrehumbert, 2000; Shraiman and Siggia, 2000). These experimental and theoretical studies have shown that small-scale tracer fluctuations have a Gaussian core and non-Gaussian tails in either turbulent or chaotic flows. The non-Gaussian tails indicate that tracer fluctuations with large concentration values are not random events and thus can not be neglected. This has important implications for nonlinear atmospheric chemistry, because nonlinear chemical reactions have reaction rates that are sensitive to large fluctuations of chemical species and not just mean chemical concentrations. A typical example is the nonlinear stratospheric ozone chemistry, in which ozone destruction rates are sensitive to large fluctuations of chlorine products (Edouard et al., 1996). An appreciation of the importance of mixing in determining ozone destruction can be obtained from Tan et al. (1998).

Hu and Pierrehumbert (2001, 2002) introduced and extended the ideas of tracer PDFs arising from idealized models to tracer mixing in realistic atmospheric flows. Although atmospheric flow is complex with the presence of transport barriers, anisotropy, and various sources and sinks, and is distinct from turbulent flows in laboratory experiments or idealized flows used in theoretical works, yet Hu and Pierrehumbert (2001) found close similarity in the PDF shape between a freely decaying tracer and those frequently reported

*E-mail: yyhu@pku.edu.cn

from experiments and theoretical works, i.e., the PDF has a Gaussian core and "fat tails". Here, "freely decaying" means that there is no external forcing or damping, and the tracer freely decays due to diffusive dissipation. For example, the moments of tracer concentration fluctuations, $\langle|\theta|^n\rangle$, decay exponentially with time, i.e., $\langle|\theta|^n\rangle \propto \exp(-\Gamma_n t)$ (Here, Γ_n is the decaying rate). The term of "fat tails" indicates that large tracer fluctuations have higher probability than normally distributed random events.

However, the real situation in the atmosphere is that most tracers are not subject to freely decaying. Instead, the variances of many long-lived (passive) tracers are maintained by various sources against diffusive dissipation. For example, tracers, such as N_2O, CH_4, and Chlorofluoro carbins (CFCs), have sources at the ground and sinks in the upper stratosphere. Their mixing ratios decrease with height in the stratosphere. Upwelling in the tropics slowly transports tracer-rich air from the troposphere, while downward motion in polar regions transports tracer-poor air from aloft. Therefore, for the kinematics of a tropospheric-source tracer on isentropic surfaces, the tropics and polar regions act as the source and sink, respectively, whereas the mid-latitude surf zones, bounded by tropical and polar mixing barriers, constitute the mixing vessels. As a result of the interaction of the source-sink and mixing, in a statistically steady state a weak zonal-mean poleward gradient of the tracer is maintained inside the mid-latitude surf zones, and the small-scale structures of the tracer fluctuate over this zonal-mean background gradient. As we shall show in the next section, the maintenance of the mean gradient provides us with a short-hand tool for studying the PDF of tracer fluctuations without directly dealing with the boundary conditions in determining how the tracer is injected into the surf zones. The purpose of the present paper is to study the PDF of a passive tracer that is driven by the lower stratospheric flow in the presence of such a "mean-gradient forcing".

The concept of such a "mean-gradient forcing" has been commonly applied to turbulence research in laboratory experiments. In Rayleigh-Benard convection experiments (Castaing et al., 1989), it is assumed that a mean vertical temperature gradient is maintained by the temperature difference between the top and bottom walls, and that temperature fluctuations produced by buoyancy forcing from the bottom wall are assumed to be generated from the mean background temperature gradient. In wind tunnel experiments (Gollub et al., 1991; Jayesh and Warhaft, 1992), it is assumed that a mean temperature gradient is maintained by a fixed temperature difference between two boundaries. In these experiments, the PDF of temperature fluctuations, deviating from the background mean temperature, is characterized by a Gaussian core and exponential tails. Theoretical studies (Yakhot et al., 1990; Shraiman and Siggia, 1994) and numerical simulations (Holzer and Siggia, 1994; Pumir, 1994) are also based on the concept of the mean-gradient forcing. In Hu and Pierrehumbert (2001), it was pointed out that mixing barriers in the subtropical and subpolar stratosphere help maintain high and low tracer concentrations in the tropics and the polar regions, respectively, and that tracer mixing in midlatitudes is like the case with an external mean-gradient forcing.

In the present paper, we study the PDFs of a N_2O-like passive tracer inside the mid-latitude surf zones, by artificially forcing the tracer in the tropics and polar regions. We shall start from theoretical considerations, with two different approaches: the Lagrangian and the conditional closure formalisms. In the former, the advection-diffusion problem is studied by evaluating the trajectory history of Lagrangian particles, and the PDF of tracer fluctuations is derived from the PDF of Lyapunov exponents. In the latter, tracer PDFs are solved from the PDF transport equation that is determined by averaging diffusive dissipation and forcing conditioned on tracer concentrations. Then, in section 3 we test the theoretical predictions by carrying out numerical simulations with an idealized random flow on a sphere and realistic stratospheric winds on the 420 K isentropic surface from the European Centre for Medium-Range Weather Forecasts (ECMWF). Details of the numerical scheme and data source can be found in Hu and Pierrehumbert (2001). In section 3.3, we compare the long-term behavior of the PDF of a freely decaying tracer with that of the forced tracer. Conclusions are presented in section 4.

2. Theoretical considerations

2.1 *The Lagrangian formalism*

The governing equation for tracer advection and diffusion is

$$\frac{\partial \Theta}{\partial t} + \boldsymbol{v} \cdot \nabla \Theta = \kappa \nabla^2 \Theta \,, \tag{1}$$

where Θ indicates the concentration or mixing ratio of a passive tracer, $\boldsymbol{v}$ is velocity and satisfies the incompressible condition $\nabla \cdot \boldsymbol{v} = 0$, and κ is diffusivity. In the theoretical discussion here, κ indicates the molecular diffusivity. In the numerical simulations, κ indicates the numerical diffusivity, and its value depends on the numerical resolution. Because diffusion is the only process that dissipates the passive tracer, dissipation is also called diffusive dissipation in the present paper.

We are generally interested in the advection-diffusion problem with two more restrictions: the large Peclet number limit, i.e., $Pe = (VL)/\kappa \gg 1$, and spatially smooth flow, that is, the velocity gradient matrix has finite eigenvalues or $|\boldsymbol{v}(\boldsymbol{x}+\boldsymbol{r}) - \boldsymbol{v}(\boldsymbol{x})| \propto r$, where V and L are the characteristic scales of velocity and eddy length, respectively, and k is the horizontal wavenumber. Here, the condition of large Peclet number requires that the advective effect dominates the diffusive effect. The condition of spatially smooth flow is used to guarantee the Lyapunov exponent, which will be used below, to be defined. As pointed out by Pierrehumbert (2000), if this condition is not satisfied, there exist singularities for velocity gradients $|\nabla \boldsymbol{v}|$, i.e., strains of the flow or the eigenvalues of $|\nabla \boldsymbol{v}|$ can be infinite, i.e., $s(t) \to \pm\infty$. Recall that Lyapunov exponents are defined by the time integral of strains, $\lambda = \frac{1}{T}\int_0^T s(t)dt$ (Pierrehumbert and Yang, 1993). A non-smooth flow would lead to undefined Lyapunov exponents over small spatial scales.

Consider a constant mean-gradient $-G = \partial\bar{\Theta}(y)/\partial y$ in the meridional direction and $0 < G \ll |\nabla\theta|$ (e.g., zonal mean tracer concentration $\bar{\Theta}(y)$ decreases with y, and local tracer gradients, $\nabla\theta$, are not swamped by the mean gradient G). Tracer fluctuations deviating from the zonal mean $\bar{\Theta}(y)$ can be defined by the relation

$$\Theta(x,y,t) = -Gy + \theta(x,y,t)\ . \tag{2}$$

Note that $\Theta = -Gy$ is a steady-state solution for Eq.(1), as the meridional component of $\boldsymbol{v}$ is zero. Substituting Eq. (2) into Eq. (1), we obtain the advection-diffusion equation for tracer fluctuations $\theta(x,y,t)$

$$\frac{\partial\theta}{\partial t} + \boldsymbol{v}\cdot\nabla\theta = \kappa\nabla^2\theta + Gv\ . \tag{3}$$

The term Gv acts as a forcing for tracer fluctuation $\theta(x,y,t)$. This forcing means that tracer fluctuations are generated by the meridional component of velocity, v, which moves tracer parcels from one latitude to another. In the steady state, the variance of tracer fluctuations, $\overline{\theta^2}$, is maintained by the balance between θ production (Gv) and diffusion ($\kappa\nabla^2\theta$) and is bounded by G^2L^2. Here, "$\overline{\cdot}$" indicates space or ensemble average of a quantity, to be distinguished from $\langle\cdot\rangle_\theta$ for conditional averages.

Under the condition of large Peclet number limit, the forced tracer field experiences two stages: (1) advection (stretching and folding) and (2) a steady state with a balance between forcing and diffusive dissipation. The two stages are separated by the dissipation time

$$t^* = \frac{1}{\lambda}\ln\left(\frac{L}{r_\mathrm{d}}\right)\ , \tag{4}$$

where λ is Lyapunov exponent, and

$$r_\mathrm{d} = \sqrt{\frac{\kappa}{\lambda}} \tag{5}$$

is the diffusive scale.

When $t < t^*$, the advective effect dominates, and the diffusive effect can be neglected. For initial condition $\theta(x,y,0) = 0$ or $\Theta(x,y,0) = -Gy$, tracer fluctuations grow with time under forcing Gv, i.e., $\theta = G\delta y$, where δy is a small displacement in the meridional direction. Because tracer parcels are driven by random forward and back motions, their net motions in the meridional direction are diffusion-like and quite slow, i.e., $\delta y \propto t^{\frac{1}{2}}$, rather than $\delta y \propto t$. Thus, the growth of tracer fluctuations is $\theta(t) \propto t^{\frac{1}{2}}$. Being driven by random motions, the probability distribution function for the meridional displacement of tracer parcels, δy, is Gaussian. Since $\theta \propto \delta y$, the PDF of tracer fluctuations at $t \leqslant t^*$ should also be Gaussian, i.e.,

$$P(\theta,t) = \frac{1}{\sqrt{2\pi ct}}\exp\left(-\frac{\theta^2}{2ct}\right)\ , \tag{6}$$

where $ct = \overline{\theta^2(t)}$ denotes the tracer variance [Result (6) is the solution of equation $\frac{\partial P(\theta,t)}{\partial t} = c\frac{\partial^2 P(\theta,t)}{\partial\theta^2}$]. Discussion on this can be found in many text books on random walk and Brownian motion, for example, Kadanoff (2000) or Pope (2000). Equation (6) yields a non-stationary distribution. As time progresses, the PDF becomes wider and wider and shifts toward high fluctuations. In the case without diffusion, large tracer fluctuations arise from random motions persistently against the mean gradient. However, one shall find below that when diffusion takes place, large tracer fluctuations are not primarily caused by such random motions.

As $t \geqslant t^*$, the diffusive effect takes place and tends to dissipate tracer fluctuations. In this stage, the growth of the tracer value is still $t^{\frac{1}{2}}$ as before, while diffusive dissipation is proportional to $\exp(-\lambda t_+)$ [see discussion in Hu and Pierrehumbert (2001, 2002)], where $t_+ = t - t^*$. The value of the tracer parcel involves with time in the way of $\theta(t) = \theta(t^*)t^{*\frac{1}{2}}_+\exp(-\lambda t_+)$. Since the decay of the tracer parcel is exponential, which is much faster than the growth, the value of the tracer will rapidly dissipate away after $t = t^*$, i.e., $\theta(t) \approx \theta(t^*)\exp(-\lambda t_+)$. Thus, t^* is the "life time" of the tracer parcel, at which the concentration value of the tracer parcel reaches its maximum value. At the statistical steady state for the whole tracer field, if all tracer parcels were determined by a single time t^*, the PDF for $t > t^*$, $P(\theta,t)$, would still be Gaussian, with variances $\overline{\theta^2} \propto t^*$, no matter how long the trajectories are integrated. However,

the fact is that each tracer parcel occupies a different t^*, which is determined by λ through Eq. (4), and thus has a different value. For example, for two tracer parcels with the same initial concentration value, the one with a smaller Lyapunov exponent has a longer "life time". In order to obtain the PDF of tracer fluctuations in the statistical steady state, the probability of t^* for all tracer parcels, $P_t(t^*)$, needs to be taken into account. This can be realized by averaging (6) over the probability of t^*, as follows,

$$P(\theta) \propto \int_0^\infty P_t(t^*) \frac{1}{\sqrt{t^*}} \exp\left(-\frac{\theta^2}{2ct^*}\right) dt^* . \quad (7)$$

$P_t(t^*)$ can be obtained from the PDF of Lyapunov exponent. Chertkov et al. (1995) showed that $P_\lambda(\lambda, t)$ has the Gaussian form, i.e.,

$$P_\lambda(\lambda, t) \propto t^{\frac{1}{2}} \exp[-\sigma_\lambda(\lambda - \bar{\lambda})^2 t] , \quad (8)$$

where $\bar{\lambda}$ is the mean Lyapunov exponents, and σ_λ measures the variance of Lyapunov exponents. Using Eq. (4) in Eq. (8) and substituting the result into Eq. (7), we have

$$P(\theta) \propto \int_0^\infty \exp\left\{-\frac{1}{t^*}\left[\sigma_\lambda \left(\ln(\frac{L}{r_\mathrm{d}})\right)^2 + \frac{\theta^2}{2c}\right] - 2\sigma_\lambda \ln\left(\frac{L}{r_\mathrm{d}}\right)\bar{\lambda} - \sigma_\lambda \bar{\lambda}^2 t^*\right\} dt^* . \quad (9)$$

The integral in Eq. (9) can be approximated using the method of steepest decent at the saddle point

$$t_c^* = \frac{1}{\bar{\lambda}} \sqrt{\left[\ln\left(\frac{L}{r_\mathrm{d}}\right)\right]^2 + \frac{\theta^2}{2\sigma_\lambda c}} . \quad (10)$$

For small θ, i.e.,

$$\frac{\theta}{\sqrt{2\sigma_\lambda c}} \ll \ln\left(\frac{L}{r_\mathrm{d}}\right) ,$$

Eq. (10) approximates

$$t_{c1}^* \approx \frac{1}{\bar{\lambda}} \ln(\frac{L}{r_\mathrm{d}}) .$$

Substitution of t_{c1}^* back into Eq. (9) yields a Gaussian core

$$P(\theta) \propto \exp\left[-\frac{1}{2c\ln\left(\frac{L}{r_\mathrm{d}}\right)} \bar{\lambda}\theta^2\right] . \quad (11)$$

For large θ, i.e,

$$\frac{|\theta|}{\sqrt{2\sigma_\lambda c}} \gg \ln\left(\frac{L}{r_\mathrm{d}}\right) ,$$

Eq. (10) approximates

$$t_{c2}^* \approx \frac{|\theta|}{\bar{\lambda}\sqrt{2\sigma_\lambda c}} .$$

Substitution of t_{c2}^* into (9) yields exponential tails

$$P(\theta) \propto \exp\left[-\left(\frac{2\sigma_\lambda}{c}\right)^{\frac{1}{2}} \bar{\lambda}|\theta|\right] . \quad (12)$$

The exponential distribution of large tracer fluctuations can also be interpreted in an alternative way. Applying Eq. (4) to Eq. (8), one can directly obtain

$$P_t(t^*) \propto \exp(-\sigma_\lambda \bar{\lambda}^2 t^*) \quad (13)$$

for large t^*, since from Eq. (8) it is required that $\lambda \ll \bar{\lambda}$ for an anomalously large t^*. Substitution of this relation into Eq. (7) yields the same result as Eq. (12). Eq. (13) indicates that the probability of these long "life times" has an exponential distribution. In other words, large tracer fluctuations have an exponential probability distribution.

Several points deserve further discussion to illustrate the physical essence of the results in Eq. (11) and Eq. (12). First, large tracer fluctuations result from small Lyapunov exponents that lead to anomalously slow diffusive mixing. This can be illustrated as follows. Since $t_{c2}^* > t_{c1}^*$ and

$$t_{c1}^* \approx \frac{1}{\bar{\lambda}} \ln\left(\frac{L}{r_\mathrm{d}}\right) ,$$

the corresponding optimal Lyapunov exponent

$$\lambda_{c2} = \frac{1}{t_{c2}^*} \ln\left(\frac{L}{r_\mathrm{d}}\right)$$

must be less than $\bar{\lambda}$. Thus, the exponential tails of $P(\theta)$ or large tracer fluctuations arise from small Lyapunov exponents or the left tail of $P_\lambda(\lambda)$. By contrast, large Lyapunov exponents, i.e., these close to and larger than the mean Lyapunov exponent, $\bar{\lambda}$, [the core part and the right tail of $P_\lambda(\lambda)$], lead to small θ and give rise of the Gaussian core of $P(\theta)$.

Second, from Eq. (12), it is clear that the exponential tails are not a function of time. This is different from the PDFs in the freely decaying case (Hu and Pierrehumbert, 2001), in which the tails becomes flatter and with time.

Third, large tracer fluctuations are not primarily caused by persistent motions against the mean background gradient. Instead, large fluctuations are associated with these tracer parcels, which have small Lyapunov exponents and move along typical trajectories. This is because the growth of tracer values from random motions, $t^{\frac{1}{2}}$, is much slower than the exponential

decay, $\exp(-\lambda t)$, after the diffusive effect takes place. In addition, since these persistent motions against the mean gradient are random events, large tracer fluctuations generated by these random motions have a Gaussian distribution, not an exponential one.

Finally, it is important to point out that in the above derivations we have assumed that the driving flow has δ-time correlation. This assumption allows us to use the relation between t^* and r_d, i.e., Eq. (4), and the PDF of Lyapunov exponents for obtaining the statistics of tracer fluctuations. If the flow has a finite-time correlation, t^* and r_d depend on the statistical properties of the strains that a tracer parcel experienced, and Eq. (4) may not be valid. This is physically addressed in Hu and Pierrehumbert (2001). Considering that the stratospheric flow has a realistic time interval of correlation, we will numerically test to what extent tracer PDFs in the stratosphere are consistent with the theories.

2.2 *The conditional closure formalism*

In this approach, the starting point is the steady state at which tracer mixing is balanced between external forcing and diffusive dissipation, regardless of detailed processes of tracer mixing from large to small scales. The PDF of tracer fluctuations is solved from the PDF transport equation that is derived from the governing advection-diffusion equation.

For general consideration, we derive the PDF transport equation with an implicit external forcing F which is independent of θ. We shall bring the specific form, Gv in Eq. (3), back to replace F when we are ready to solve the equation. With forcing F, Eq. (3) is rewritten as

$$\frac{\partial \theta}{\partial t} + \boldsymbol{v} \cdot \nabla \theta = \kappa \nabla^2 \theta + F \; . \tag{14}$$

There are many ways to derive the PDF transport equation of motion in the presence of forcing (see Yakhot et al., 1990; Ching and Kraichnan, 1998; Pierrehumbert, 2000). In this study, we derive the PDF equation from the area-tracer relationship. This method was developed by Nakamura (1996) for quantifying effective diffusivity in two-dimensional flows and has proved to be very useful for diagnosing tracer mixing and mixing barriers in the stratosphere (Allen et al., 1999; Haynes and Shuckburgh, 2000). By following Nakamura (1996), an area bounded by a contour of θ is defined as

$$A_\theta(\theta, t) \equiv \iint_{\theta_\mathrm{min} \leqslant \theta^* \leqslant \theta} dxdy \tag{15}$$

where θ^* is a descriptor of tracer contours. $A_\theta(\theta, t)$ indicates the area between contours θ_min and θ at time t. In the area coordinate, the PDF of tracer θ is defined as

$$P(\theta, t) \equiv \frac{\partial A_\theta}{\partial \theta} \; , \tag{16}$$

since the probability of sampling a value between θ and $\theta + \delta\theta$ is the fraction of the area bounded by the two contours $\theta^* = \theta$ and $\theta^* = \theta + \delta\theta$. The average of any quantity "$\cdot$" over the area enclosed by two infinitesimally adjacent θ-contours is defined as

$$\langle \cdot \rangle_\theta \equiv \frac{\partial}{\partial A_\theta} \iint_{\theta_\mathrm{min} \leqslant \theta^* \leqslant \theta} (\cdot) dxdy \; . \tag{17}$$

This θ-area-averaged $\langle \cdot \rangle_\theta$ is called a conditional quantity, since it is an average conditioned on θ (In practice, to obtain meaningful statistics, a sufficiently large $\delta\theta$ is necessary for sampling enough independent realizations for area averages). With these, we can derive the PDF transport equation following the method of Nakamura (1996). The equation is

$$\frac{\partial}{\partial t} P(\theta, t) = -\frac{\partial^2}{\partial \theta^2} [\langle \kappa (\nabla \theta)^2 \rangle_\theta P] - \frac{\partial}{\partial \theta} \langle F \rangle_\theta P \; . \tag{18}$$

In this equation, $\langle \kappa |\nabla \theta|^2 \rangle_\theta$ is the conditional dissipation, and $\langle F \rangle_\theta$ is the conditional forcing. Both are conditioned on θ. For convenience, the former is indicated by $\langle D \rangle_\theta$.

When external forcing is balanced by diffusive dissipation, the tracer field reaches a steady state. The PDF equation then becomes,

$$\frac{\partial^2}{\partial \theta^2} [\langle D \rangle_\theta P] + \frac{\partial}{\partial \theta} [\langle F \rangle_\theta P] = 0 \; . \tag{19}$$

Integrating Eq. (19) twice, we obtain a general solution for the tracer PDF

$$P(\theta) = \frac{C}{\langle D \rangle_\theta} \exp \left(- \int_{\theta_\mathrm{min}}^{\theta} \frac{\langle F \rangle_\theta}{\langle D \rangle_\theta} d\theta^* \right) \; , \tag{20}$$

where C is a normalization constant. Note that we have assumed the integral constant of the first integral equals zero. It is equivalent to $\partial A_\theta / \partial t = 0$, meaning that not only the PDF but also the areas enclosed by any θ-contours are steady. Eq. (20) simply states that the tracer PDF is determined by conditional dissipation and forcing. If the two conditional variables are known, solution (20) can be evaluated explicitly. The general solution of the PDF for a forced tracer is similar to the Ching-Kraichnan formula for a decaying tracer [see Eq. (7) in Hu and Pierrehumbert (2001)], except that the conditional diffusion in their formula is replaced by conditional forcing with a negative sign. We shall see that what makes the PDF of a forced tracer different from that of a decaying tracer is the difference in the conditional dissipation between the two cases.

For conditional forcing, using the specific forcing $F = Gv$, we have

$$\langle F\rangle_\theta = G\langle v\rangle_\theta \,. \tag{21}$$

Thus, the problem of the conditional forcing is reduced to that of conditional velocity $\langle v\rangle_\theta$. In a steady state, multiplying (3) by θ and taking spatial average yield

$$\kappa\overline{(\nabla\theta)^2} = G\overline{v\theta}\,. \tag{22}$$

Since the left-hand side is always positive, for N_2O-like tracers, $G > 0, \overline{v\theta} > 0$ in the Northern Hemisphere, and $G < 0, \overline{v\theta} < 0$ in the southern hemisphere. In other words, the mean tracer flux is always toward the poles. This means that in the northern (southern) hemispherethe averaged velocity over the area where $\theta > 0$ is positive (negative), while over the area where $\theta < 0$, it is negative (positive). Assuming symmetry in the tracer statistics between positive and negative θ, we can expect an odd-symmetry, $\langle v\rangle_\theta = -\langle v\rangle_{-\theta}$. Such a relationship can also be directly deduced from Eq. (20). Assume that $P(\theta)$ and $\langle D\rangle_\theta$ are both symmetric about $\theta = 0$. $\langle F\rangle_\theta$ must be anti-symmetric with respect to $\theta = 0$, i.e., $\langle v\rangle_\theta = -\langle v\rangle_{-\theta}$, and local Taylor expansion of $\langle v\rangle_\theta$ at $\theta \to 0$ yields a linear relationship between $\langle v\rangle_\theta$ and θ

$$\langle v\rangle_\theta = q\theta\,, \tag{23}$$

where q is constant (In the next section, we will show that this local linear relationship is actually valid for an appreciable range of θ). Then, we have

$$\langle F\rangle_\theta = Gq\theta = K\theta\,, \tag{24}$$

where $K = Gq$.

Conditional dissipation $\langle D\rangle_\theta = \langle\kappa(\nabla\theta)^2\rangle_\theta$ must be a positive even function of gradients since it is the conditional average of squared tracer gradients. We can use the first two orders of an even function of θ,

$$\langle D\rangle_\theta = a + b|\theta|\,, \tag{25}$$

$$\langle D\rangle_\theta = a + b\theta^2\,, \tag{26}$$

where a and b are both constants, as test functions for the conditional dissipation. We will see in numerical simulations below that slope b can be different for $\theta > 0$ and $\theta < 0$.

Having known $\langle F\rangle_\theta$ and $\langle D\rangle_\theta$, we are able to obtain an explicit steady-state PDF solution. For small $|\theta|$, i.e, $|\theta| \ll a/b$, substituting $\langle D\rangle_\theta \approx a$ and Eq. (24) to Eq. (20), we have

$$P(\theta) \propto \exp\left(-\frac{K}{2a}\theta^2\right)\,. \tag{27}$$

For $|\theta| \gg a/b$, substitution of Eq. (24) and Eq. (25) into Eq. (20) yields

$$P(\theta) \propto (a + b|\theta|)^{\frac{Ka}{b^2}-1}\exp\left(-\frac{K}{b}|\theta|\right)\,. \tag{28}$$

Since the exponential term in Eq. (28) is the dominant part, the PDF has exponential tails. $|\theta| = a/b$ is the cross-over point between the Gaussian core and exponential tails. Ratio $\frac{K}{b}$ is the fall-off rate of the PDF. If we choose relation Eq. (26) for conditional dissipation, for $\theta^2 \ll a/b$, we have a Gaussian core, same as Eq. (27). For $\theta^2 \gg a/b$, the solution is

$$P(\theta) \propto \frac{1}{(a + b\theta^2)^{1+\frac{K}{2b}}}\,, \tag{29}$$

which is the same as Sinai and Yakhot's solution for a decaying tracer (Sinai and Yakhot, 1989), except that here K is the slope of condition forcing, instead of the slope of conditional diffusion. This PDF has algebraic tails which are flatter than exponential.

The parabolic relationship for conditional dissipation was first suggested by Eswarson and Pope (1988) based on their numerical simulations for a decaying tracer in a turbulent flow. Sinai and Yakhot (1989) used this parabolic relationship and obtained solution (29). This parabolic shape of conditional dissipation was also observed for a decaying passive tracer in a lattice model (Pierrehumbert, 2000). Interestingly, the parabolic relation was never observed in a wind tunnel or Rayleigh-Benard convection experiments (Jayesh and Warhaft, 1992; Ching, 1996). Instead, these experiments all reported a linear relation. It is presum-

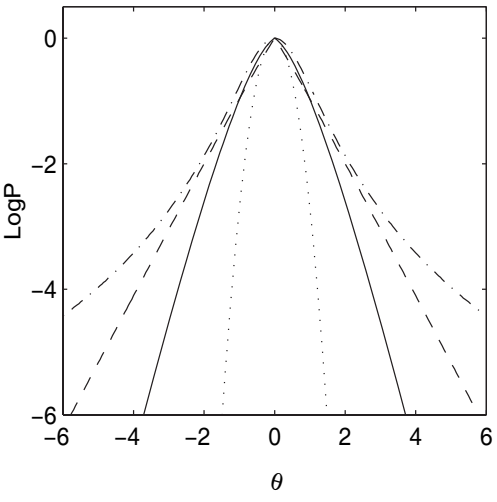

Fig. 1. Comparison of PDFs from Eqs. (28) and (29). The solid-curve is for Eq. (28), and the dashed-dotted-curve is for Eq. (29), with $a = 1.0, b = 0.8$, and $K = 5.0$. The dashed-curve is also for Eq. (28), with different parameters $a = 1.0$, $b = 2.0$, and $K = 5.0$ the dotted-curve is a Gaussian distribution.

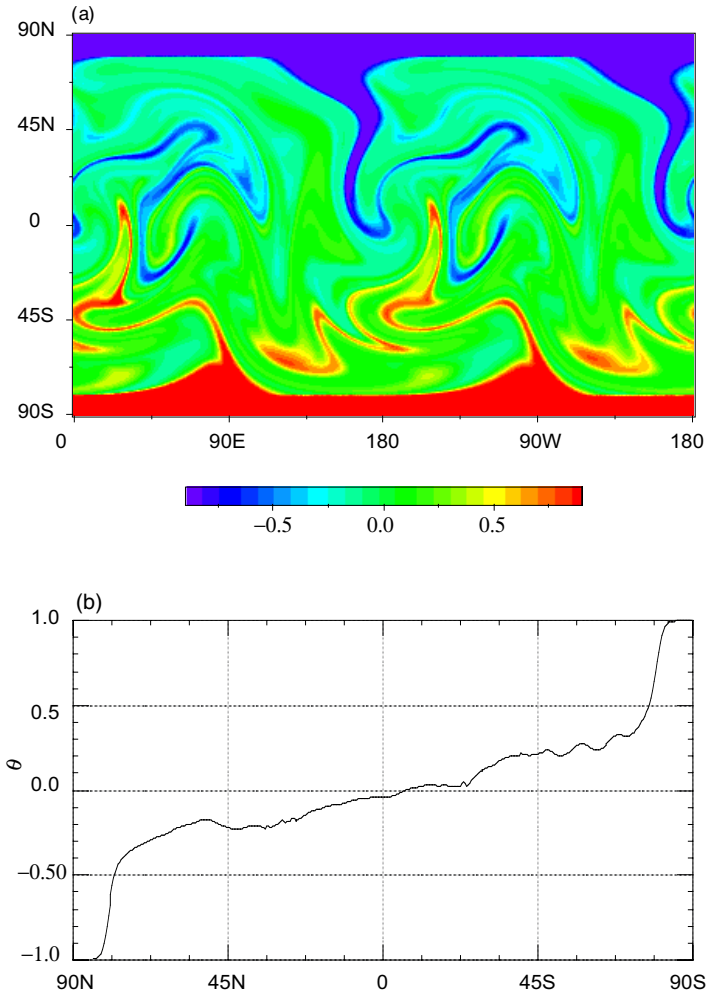

Fig. 2. (a) Snapshot of an artificially forced passive tracer driven by an idealized random flow on a sphere at day 40, and (b) zonal-mean profile of tracer concentration corresponding to the snapshot.

ably because these experiments present the case with forcing. Based on both laboratory experiments and the most recent numerical results, it appears that the parabolic approximation for conditional dissipation only represents the asymptotic behavior for a decaying tracer at sufficiently long times. By contrast, Eq. (25) is an approximation for a forced tracer in which conditional dissipation does not change any more once the steady state is reached. In Hu and Pierrehumbert (2001), we also found a linear relation for a decaying tracer in the case of zonal mixing in a two-month simulation with stratospheric winds. Later, we will show that for longer-time simulations the conditional dissipation in our decaying case evolves from linear to parabolic.

To distinguish the PDF shapes between solutions (28) and (29), we plot the solutions in Fig. 1. The dotted curve is a Gaussian distribution for comparison. The solid curve represents solution (28), which shows a small Gaussian-like core and exponential tails. The dashed-dotted curve is for solution (29). It shows concave tails, flatter than exponential. The dashed curve is also for solution (28), however, with a greater slope for conditional dissipation. In this case, the exponential tails are more dominant, while the Gaussian core is not evident. The numerical results below show that solution (29) is for a decaying tracer, not adequate for the case with forcing.

3. Numerical results

3.1 *Tracer PDF in an idealized random flow*

To test the theoretical predictions, we first carry out a numerical simulation in which a forced passive tracer is driven by a large-scale random flow on a sphere. The streamfunction of the random flow is con-

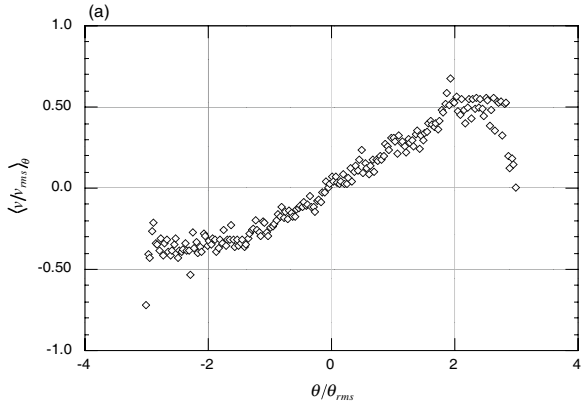

(a)

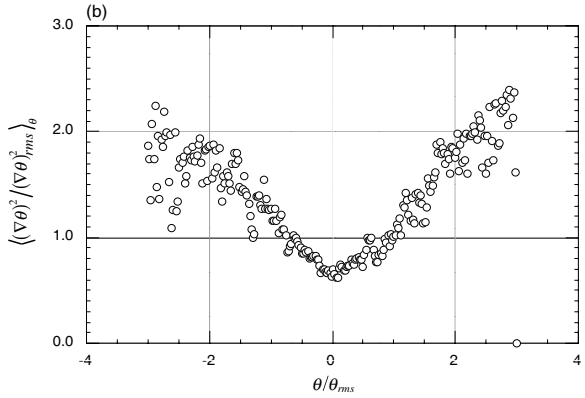

(b)

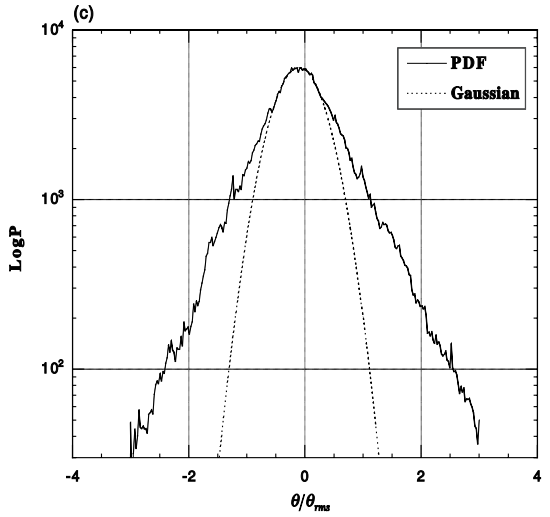

(c)

Fig. 3. PDF and conditional quantities for a forced passive tracer in the random flow. (a) Conditional velocity, (b) conditional dissipation, and (c) PDF of tracer fluctuations. The vertical axis in (c) is in logarithm, and the horizontal axis is normalized by the root-mean-square (rms) of the tracer fluctuations.

structed using spherical harmonics, i.e.,

$$\psi(\Lambda,\phi,t) = \sum_{n=0}^{N} \sum_{m=-n}^{n} \psi_{m,n}(t) Y_{m,n}(\Lambda,\phi) \;, \qquad (30)$$

where $\psi, \psi_{m,n}(t), \Lambda, \phi$, and $Y_{m,n}$ indicate streamfunction, spectrum amplitude, longitude, latitude, and spherical harmonic, respectively. To make the flow random, we add a random zonal phase $\delta\Lambda(t) \in [0, 2\pi]$ to amplitude $\psi_{m,n}(t)$

$$\psi_{m,n}(t) = B e^{i\delta\Lambda(t)} \;, \qquad (31)$$

where $B = 6R$, and R is the earth's radius. The random phase is updated each 6 hours. Since we are concerned with tracer mixing in a large-scale random flow, we pick the first few modes of spherical harmonics, $n = 0, \ldots, 6$, and $m = -6, \ldots, 6$, using triangular truncation. Note that this random flow is unrealistic. There are no jets or barriers to mixing, though mixing across the equator is relatively weak.

A passive tracer is initially arranged on the sphere with $\Theta_0 = -\sin(\phi)$. Subsequently, tracer concentration values inside the polar regions are fixed, with 1.0 for 80°–90°S and −1.0 for 80°–90°N. Note that the tracer is forced in such a way to test whether the mean-gradient model works and whether the PDF of the forced tracer is consistent with the theoretical predictions. In the simulation with ECMWF winds below, the tracer is forced in a more realistic way. Figure 2a shows a snapshot of the tracer field in the random flow (t=40 days). The snapshot shows that tracer filaments are stretched out from polar regions into lower latitudes, where the filaments cascade into smaller scales and will eventually disappear due to diffusive dissipation. New filaments are generated as the old ones are dissipated away. The repeated injection of the polar tracer maintains tracer variances in the mixing zone. Figure 2b shows the zonal-mean profile of the tracer field in the snapshot. The weak slope between 70°S and 70°N indicates the existence of the mean northward meridional gradient.

Figure 3a shows the scatter of conditional velocity between 60°S and 60°N corresponding to the snapshot. The plot clearly shows a linear relationship between the conditional velocity and normalized tracer fluctuations $\theta/\theta_{\rm rms}$, consistent with the proposed relation of Eq. (24). The linear approximation of the conditional velocity appears to be valid only within the range of $-2.0 < \theta/\theta_{\rm rms} < 2.0$. Beyond this range, the conditional velocity tends to be saturated. This behavior could be related to some tracer filaments near the forcing boundaries, where motions of tracer parcels may not be random. These filaments have anomalously large concentration values, but are rare and unimportant. Figure 3b shows the scatter of the conditional

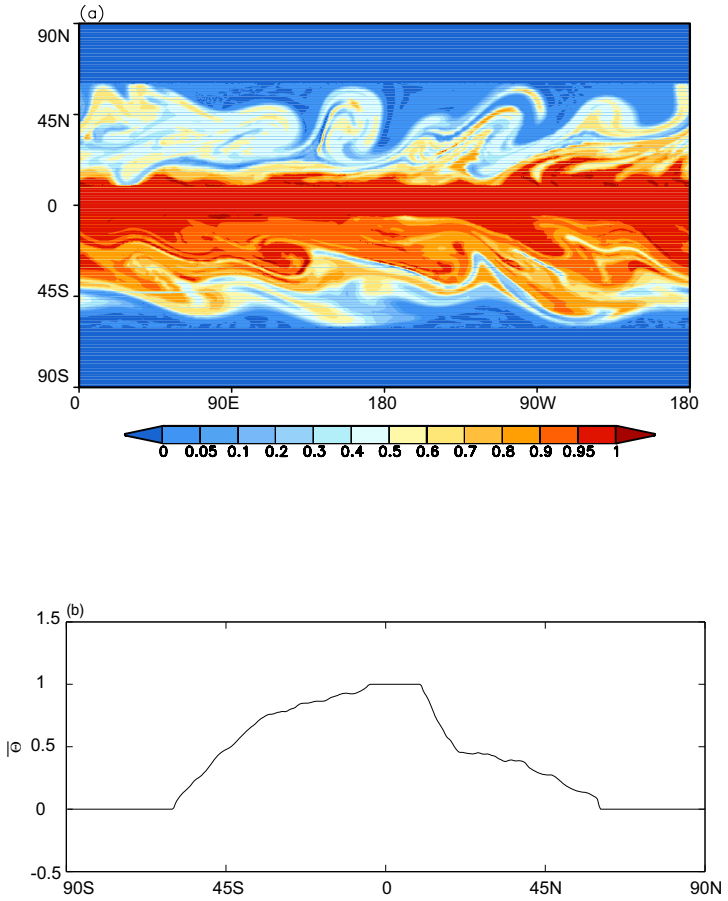

Fig. 4. Snapshot of a forced tracer driven by ECMWF winds, September 10, 1992. (a) Mixing map and (b)zonal-mean profile of tracer concentration.

dissipation, which increases approximately linearly with $|\theta|$. This suggests that the relation in Eq. (25) is more representative of conditional dissipation than that in Eq. (26). The linear relation of the conditional dissipation is valid over the range of $-2.5 < \theta/\theta_{\rm rms} < 2.5$. Large fluctuations at the ends of the scatter plot are associated with filaments near the forcing boundaries. Figure 3c shows the PDF of tracer fluctuations at day 40. The solid curve is the PDF of tracer fluctuations, and the dotted-curve is a Gaussian fitting-curve for comparison. The plot clearly shows a small Gaussian core and exponential tails. The PDF is consistent with solution (28), but appears not to agree with the algebraic solution in Eq. (29).

3.2 *Tracer PDFs in ECMWF winds*

In this section, we test whether the above theoretical predictions can be applied to understanding passive tracer mixing in the stratospheric midlatitudes. In the following simulation, a passive tracer, with initial condition of $\Theta_0 = \cos(\phi)$, is driven by ECMWF winds on the 420 K isentropic surface. The simulation starts from 1 July 1992. To set the forcing, we keep tracer concentration fixed inside the tropical "reservoir" zone which is a zonal band between 5°S and 10°N. Tracer concentrations inside both polar regions, 60°–90°S and 60°–90°N, are also fixed. It is noted that the effect of the artificial forcing does not take place until about day 40. Before that, the initial condition dominates.

Figure 4a shows the tracer field at day 70. In the Southern Hemisphere, the midlatitudes are filled with tracer filaments that are stretched out from both the tropics and the polar region. Because of the strong westerly jet stream in the Southern Hemisphere, these tracer filaments are nearly zonally oriented. In the Northern Hemisphere, tracer filaments stretched out from the tropics to midlatitudes are also evident. However, the leakage from the tropics is much weaker in the Southern Hemisphere, indicating the existence of a mixing barrier in the Northern-Hemisphere subtropics. Because of the relatively weak leakage, tracer filaments in the northern midlatitudes are not so dominant as

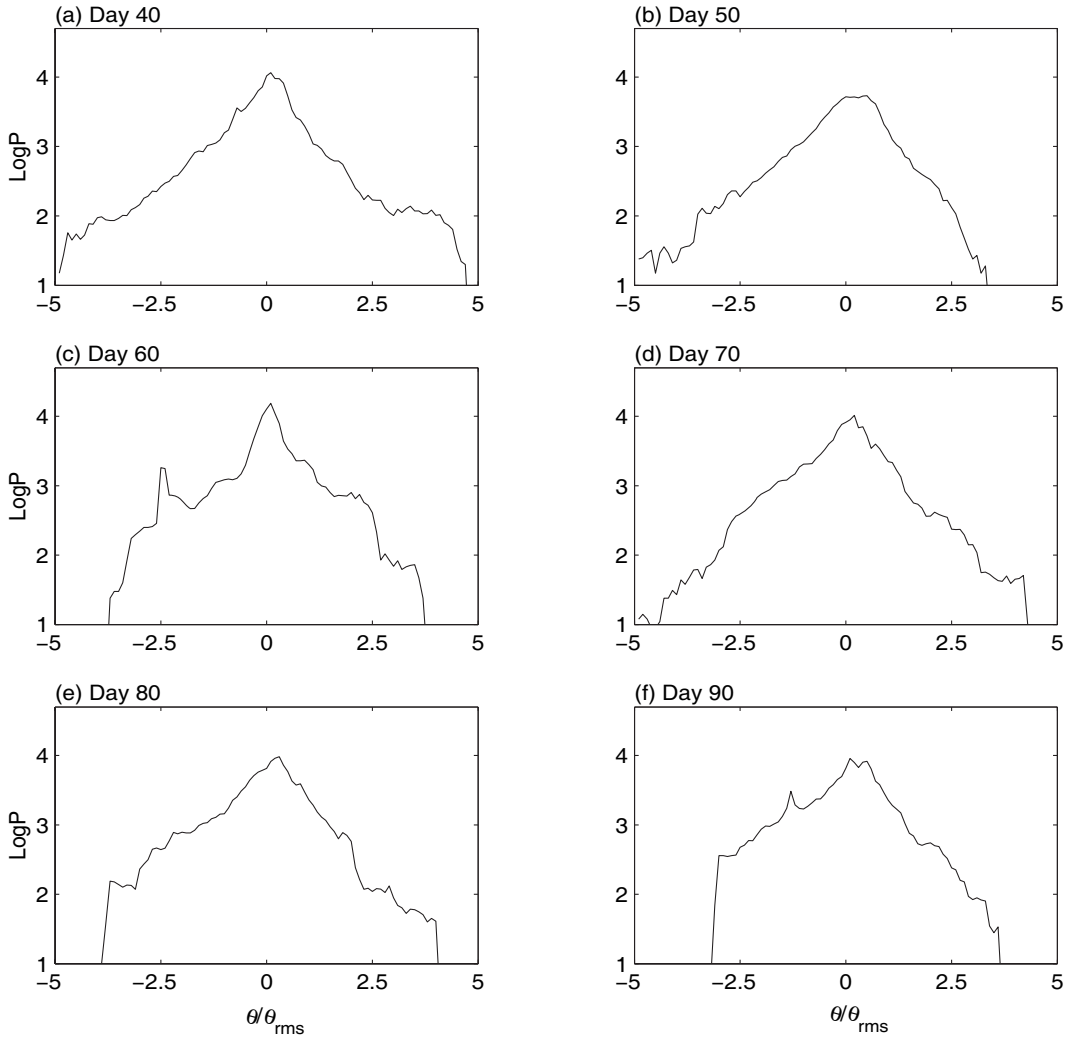

Fig. 5. PDFs of tracer fluctuations in the Southern Hemisphere. The PDFs are calculated over 60°–5°S.

that in the southern midlatitudes, implying different tracer statistics between the two hemispheres. Figure 4b illustrates the profile of zonal-mean tracer concentration ($\overline{\Theta}$). The profile is qualitatively similar to the zonal-mean profiles of tropospheric-source gases such as N_2O (Nakamura et al., 1999). In the Northern Hemisphere, a zone with sharp meridional gradients between 10°N and 20°N is indicative of the subtropical mixing barrier. A zone with a relatively weak meridional gradient between 20°N to 60°N is the mixing region of high-concentration tracer from the tropics with low-concentration from high latitudes. In the Southern Hemisphere, there is no such a zone with sharp meridional gradients in the subtropics, suggesting the lack of a strong mixing barrier between the tropics and southern midlatitudes. The mean gradient in the Southern Hemisphere is not exactly linear with latitude. However, as shown below, this seems not to affect the properties of conditional forcing very much. In the following, the PDFs, conditional dissipations, and conditional forcing are calculated over 60°–5°S and 20°–60°N for the Southern and Northern Hemispheres, respectively. The zonal-mean tracer concentration, $\overline{\Theta}$, is removed for these calculations.

Figure 5 shows the PDFs in the Southern Hemisphere. At day 40, the PDF exhibits concave behavior, indicating that the PDF tails are flatter than exponential. At day 50, the PDF shows exponential tails. By day 60, the PDF again shows concave behavior. It appears that during this period the PDF tails vacillate between exponential and flatter than exponential presumably because tracer mixing in the Southern Hemisphere during this period has not reached a steady state yet. As mentioned before, the artificial forcing becomes effective around day 40. It takes time to reach the balance between forcing and dissipation. At day 70, 80, and 90, the PDFs all show exponential tails, consistent with Eq. (28). Note that because the leak-

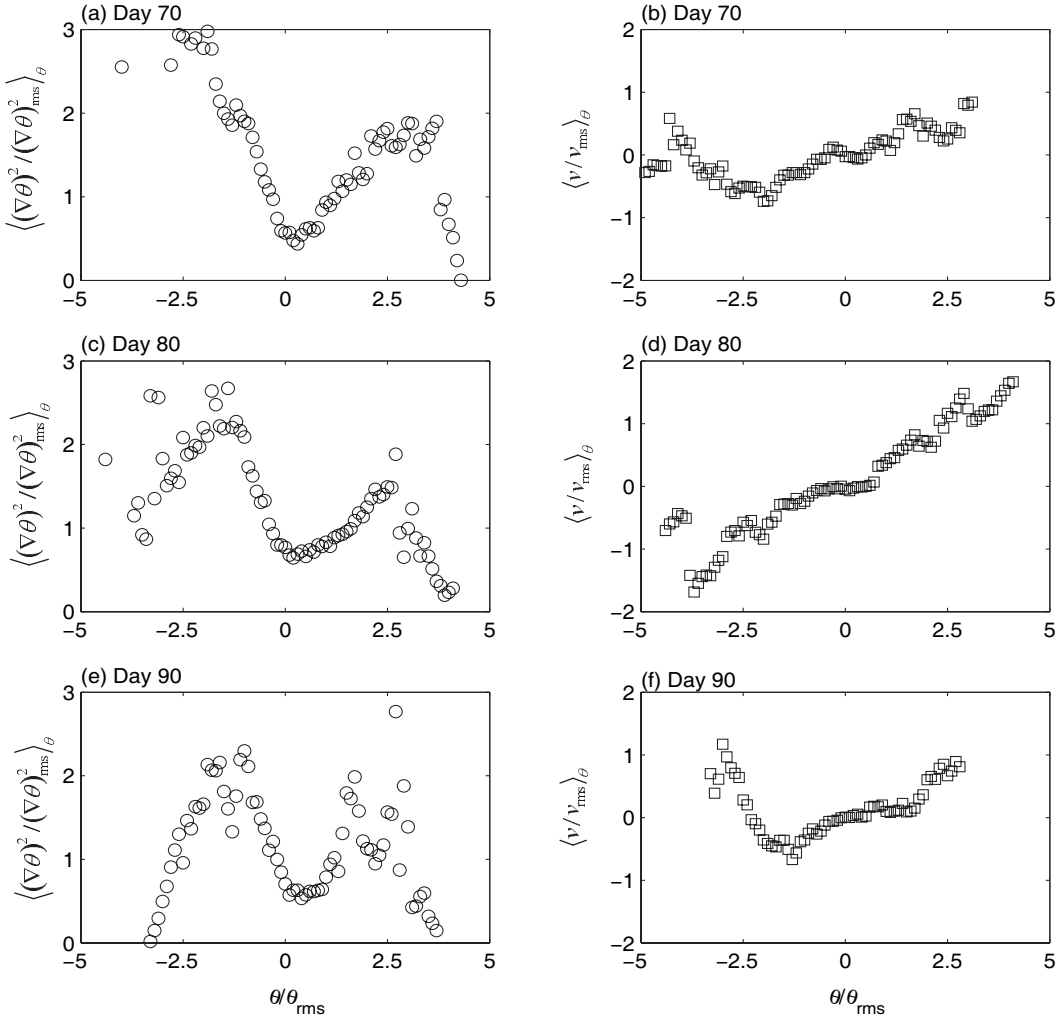

Fig. 6. Conditional dissipation and conditional velocity in the Southern Hemisphere. The plots on the left side are for conditional dissipation, and the plots on the right side are for conditional velocity.

age of tracer from both the polar and tropical regions are not continuous, but intermittent due to occasional planetary wavebreaking, the PDF shapes are not exactly time-invariant. In particular, the remote tails vary from day 70 to day 80 and 90. Thus, one may consider the balance between forcing and dissipation as a quasi-steady state.

Figure 6 shows scatter plots of conditional dissipation and conditional velocity in the Southern Hemisphere. At day 70, the scatter plot of conditional dissipation shows a compact linear relation for both branches, with large fluctuations for $\theta/\theta_{\rm rms} > 2.5$. The scatter plot of conditional velocity at day 70 also shows a linear relation for $\theta/\theta_{\rm rms} > -2.5$. Note that in the Southern Hemisphere, positive tracer fluctuations are carried southward by poleward (negative) winds, i.e., $\overline{v\theta} < 0$. For consistency with the Northern Hemisphere, the sign of the conditional velocity in Figs. 6b, d, and f is reversed. At day 80 and 90, conditional velocity and the left branch of conditional dissipation are also linear functions of θ, while the right branch of conditional dissipation exhibits slightly nonlinear behavior. In general, the scatter plots of conditional velocity and dissipation show reasonable consistency with Eqs. (24) and (25), respectively. Especially, the expected linear relation for conditional forcing in Eq. (24), which is based on local Taylor expansion at $\theta \to 0$, seems to be valid over a much wider range. According to Eq. (20), these linear conditional quantities yield exponential PDFs, consistent with the PDFs in Figs. 5e and f.

While the conditional velocity is nearly symmetric at these days, the conditional dissipation is not. The slopes of the left branches ($\theta < 0$) are generally steeper

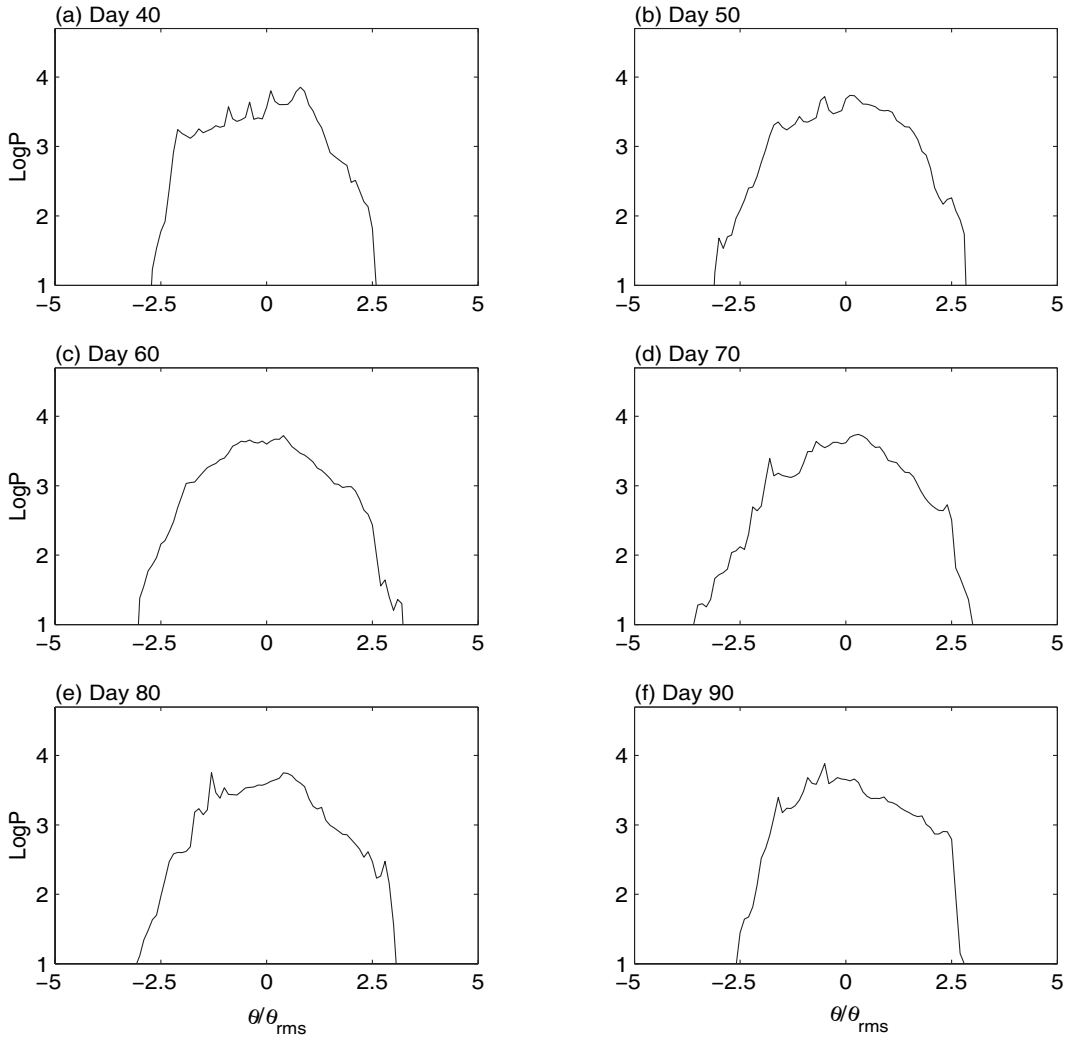

Fig. 7. PDFs of tracer fluctuations in the Northern Hemisphere. The PDFs are calculated over 20°–60°N.

than that of the right branches ($\theta > 0$). Since K/b is the fall-off rate of PDF tails, a smaller b of the right branch of conditional dissipation should have lead to a steeper right PDF tail. Indeed, at day 80 and 90 the PDFs exhibit skewness, with the right tail falling faster. At day 70, the skewness is not so profound as it was at day 80 and 90.

The scatter plots of conditional dissipation and velocity show either an inconsistency with the linear approximation or with anomalously large fluctuations beyond the range of $-2.5 < \theta/\theta_{\rm rms} < 2.5$. The anomalously large fluctuations of the conditional quantities correspond to the PDF skirts in Fig. 5. For example, at day 90 the sharp increase in conditional velocity and the rapid decrease in conditional dissipation for $\theta/\theta_{\rm rms} < -2.0$ lead to a positive and extremely large K/b, which gives rise of the skirt at the left tail of the tracer PDF. Since the anomalous behavior in conditional velocity and dissipation corresponds to large tracer fluctuations and velocities, but small tracer gradients, it is presumable that the anomalous behavior is associated with tracer filaments newly stretched out from the tropics or the polar region due to anomalously large meridional motions. Because these tracer filaments have not become sufficiently thin, tracer gradients and corresponding conditional dissipation are anomalously small. This suggests that the linear approximation for both conditional dissipation and velocity is valid only for a limited range. As shown below, the range is even narrower in the Northern Hemisphere. The phenomenon of PDF skirts are also observed in turbulence experiments as sampling is close to lateral boundaries (Lane et al., 1993).

The PDFs in the Northern Hemisphere are different from those in the Southern Hemisphere. Figure 7 shows the time variation of PDFs in the Northern Hemisphere. At day 40, the PDF shape is very irregular, i.e., neither Gaussian nor exponential. At days

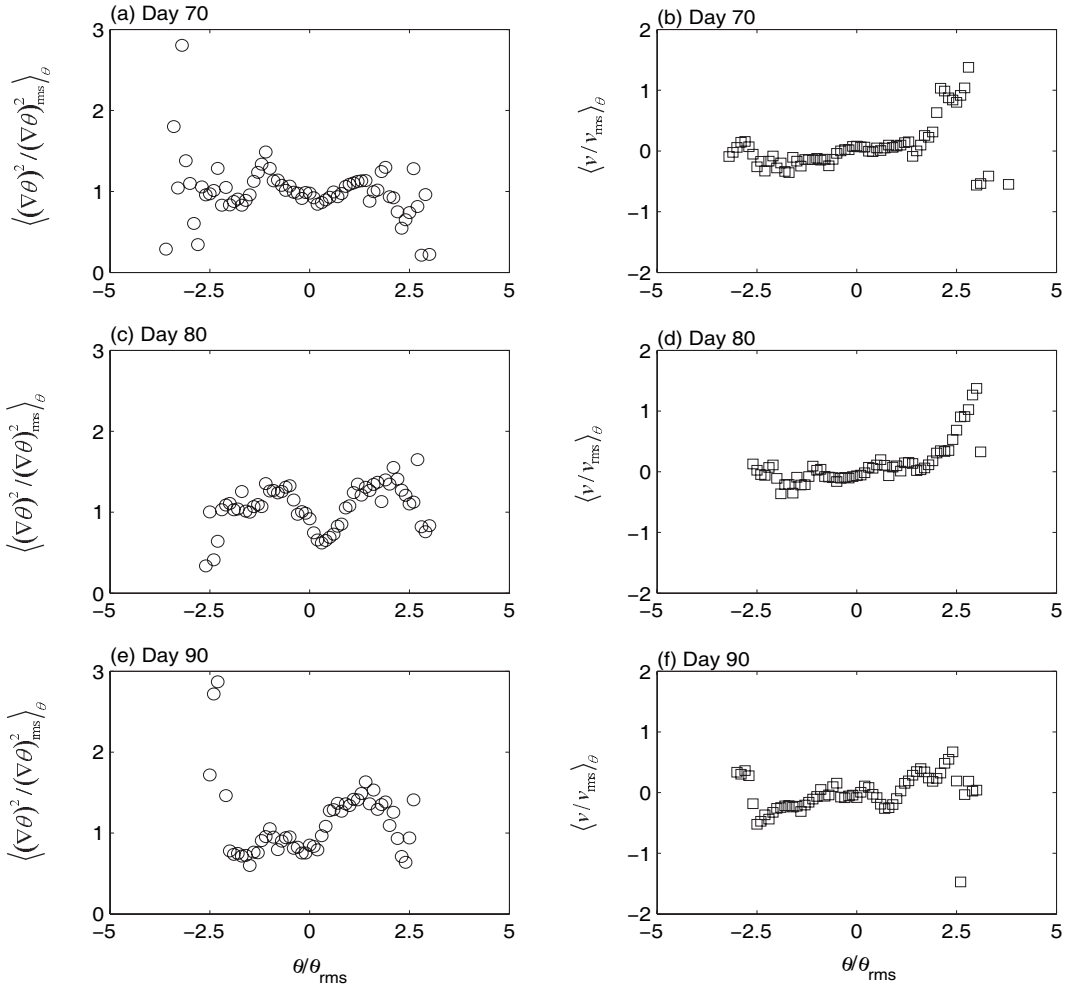

Fig. 8. Conditional dissipation and conditional velocity in the Northern Hemisphere. The plots on the left side are for conditional dissipation, and the plots on the right side are for conditional velocity.

50 and 60, the PDFs are probably close to Gaussian. The PDF at day 70 appears to have a broad Gaussian core, with the left tail close to exponential distribution. By days 80 and 90, the PDFs show short exponential tails, with deep and sharp-cut skirts. Scatter plots of conditional dissipation and velocity in the Northern-Hemisphere at days 70, 80, and 90 are shown in Fig. 8. On the one hand, the conditional quantities show compact linear relations, like that in the Southern Hemisphere. The linear approximations are valid in a narrower range than in the Southern Hemisphere, roughly within $-1.5 < \theta/\theta_{\rm rms} < 1.5$ for conditional dissipation. On the other hand, the conditional quantities in the Northern Hemisphere have much shallower slopes than in the Southern Hemisphere. The weaker conditional dissipation is due to the weaker zonal-mean tracer gradient in the northern surf zone, and the weaker conditional velocity reflects the coincidence of relatively weak meridional velocity or wave activity in the Northern (summer) Hemisphere. For Northern Hemisphere, the fall-off rate is $K/b \approx 0.5$, while for Southern Hemisphere, it is $K/b \approx 1.25$ at day 80. Thus, the PDF tails fall much faster in the Southern Hemisphere than in the Northern Hemisphere.

The differences in PDFs between the two hemispheres can also be interpreted in terms of finite time Lyapunov exponents (FTLEs). As discussed in section 2.1, the tails of the tracer PDFs are determined by small Lyapunov exponents. In Figs. 3a and b of Hu and Pierrehumbert (2001), it was shown that the left tail of the FTLE PDF consists of much smaller FTLEs in the Northern Hemisphere than in the Southern Hemisphere. These small FTLEs lead to large tracer fluctuations (relative to the $\theta_{\rm rms}$ in the northern surf zone). Thus, the weaker fall-off rate of the tracer PDF tails in the Northern Hemisphere is consistent

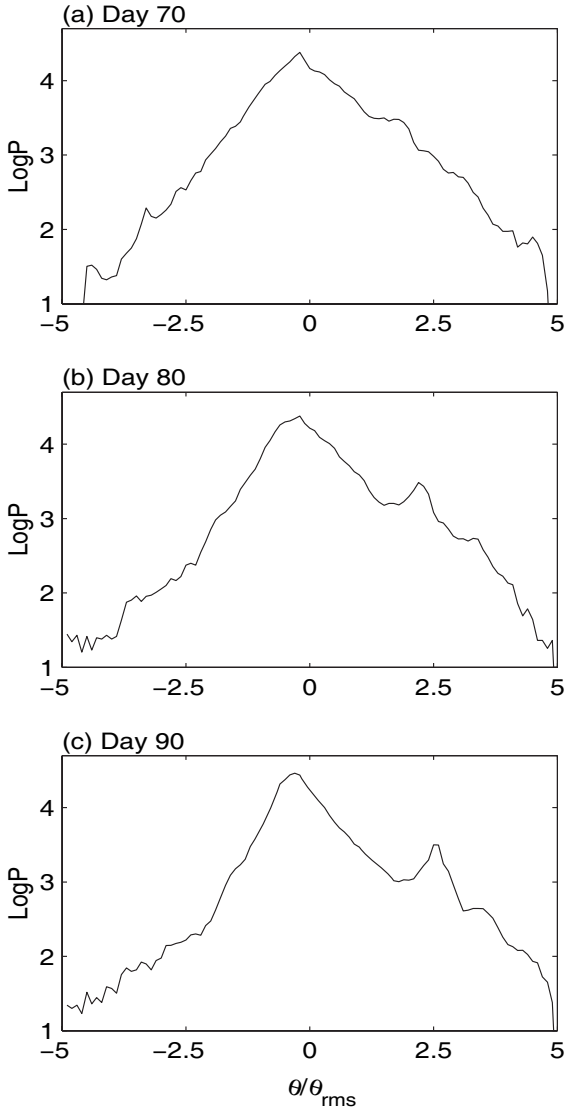

Fig. 9. Time variation of PDFs for a decaying tracer. The PDFs are calculated over the globe.

with the corresponding FTLE PDFs, suggesting the dependence of tracer statistics on Lyapunov exponent statistics. The slower fall-off rate in the Northern Hemisphere is also consistent with solutions (11) and (12), in which a smaller $\bar{\lambda}$ leads to a slower fall-off rate of PDF tails, assuming that other variables are the same. From Figure 3a and b of Hu and Pierrehumbert (2001), one can find that the mean FTLE, $\bar{\lambda}$, is smaller in the Northern Hemisphere than in the Southern Hemisphere (about 2.5 d^{-1} vs. 3.0 d^{-1}). In addition, the PDFs in Northern Hemisphere does not seem to be very consistent with the theoretical expectation. The deviation is presumably because strains in the Northern Hemisphere in these months have too long correlation times. It is known that in these months wave activity in the Northern Hemisphere is relatively weak, which leads to relatively slowly varying strains. The correlation time of the Northern Hemisphere flow may be too long to fit the condition of δ-time or short finite-time correlation for theoretical results in Eqs. (11) and (12). This may be the essential difference of tracer PDFs between the two hemispheres.

3.3 *Long-term behavior of a decaying tracer*

In Hu and Pierrehumbert (2001), we noted that for a freely decaying passive tracer, the PDF tails vary with time, and that after sufficiently long time the PDF tails will become flatter than exponential. We mentioned that the two-month (July–August) simulation might not have been long enough to illustrate such a time-dependent behavior. Here, to demonstrate the time-dependent behavior of the PDF tails over a longer period and to compare it with that of the forced tracer, we extend the two-month run of the zonal-mixing case in Hu and Pierrehumbert (2001) to three months.

The time variation of PDF shapes in the first two months has been discussed in Hu and Pierrehumbert (2001) (see their Fig. 8), in which the PDF tails at days 40 and 60 are close to exponential. Here, Fig. 9 shows the PDFs by days 70, 80, and 90. One can see that at day 70 the PDF tails still exhibit exponential behavior. By day 80, the left tail becomes concave, flatter than exponential. By day 90, the concave behavior of the left tail becomes more pronounced. These are consistent with the prediction that the PDF tails of a decaying tracer become flatter and flatter with time. The "little peak" on the right tail at day 90 is due to the existence of mixing barriers. In Hu and Pierrehumbert (2001), we pointed out that the zonal mixing case would eventually become similar to the meridional-mixing case because mixing barriers separate the globe into several regions, such as midlatitude surf zones, the tropics, and polar regions, which have very different mixing properties. When large-scale tracer variations in the zonal direction are smoothed out in these regions, tracer variations in the meridional direction between these zones become dominant, and the unimodal PDF evolves into a multimodal PDF, with each peak indicating a mixing zone just like that in Fig. 13 in Hu and Pierrehumbert (2001).

A question is what causes the difference in the long-term behavior of the PDF tails between the forcing and decaying cases. Recall that the PDF of a decaying tracer is determined by conditional dissipation and diffusion [see Eq. (7) in Hu and Pierrehumbert (2001)]. The time variation of the PDFs in Fig. 9 should be reflected in time variations of the conditional quantities. Figure 10 shows scatter plots of the conditional quantities. At day 70, the conditional dissipation exhibits

a linear relationship. At day 80, the scatter plot of the conditional dissipation exhibits a parabolic shape. By day 90, the parabolic shape becomes more dominant. The variation of the conditional dissipation from linear to parabolic means that as time progresses tracer gradients conditioned on large tracer fluctuations become much larger than those conditioned on smaller tracer fluctuations.

The scatter plots of the conditional diffusion demonstrate a linear relationship with θ (Figs. 10b, d, and f). While the conditional dissipation varies with time, the nearly linear relationship of the conditional diffusion seems to remain unchanged with time, though the slope of the linear approximation changes. This is particularly true at days 70 and 80. At day 90, the conditional diffusion for $\theta > 0$ appears not to be linear with θ. This is actually consistent with the little peak at the right PDF tail at $\theta/\theta_{\rm rms} \approx 2.5$. Since the linear property of conditional diffusion is time invariant, the time variation of the PDF tails from exponential to flatter than exponential arises from the changes in conditional dissipation. According to Eq. (7) in Hu and Pierrehumbert (2001), at day 70 the linear conditional dissipation, together with the linear conditional diffusion, yields a PDF with exponential tails, and at days 80 and 90, the parabolic conditional dissipation and the linear conditional diffusion lead to an algebraic PDF. Thus, the difference in the long-term behavior of PDF tails between the forcing and decaying cases arises from the difference in conditional dissipations. In the decaying case, the conditional dissipation evolves from linear to parabolic with time. It leads to time-dependent PDFs with tails becoming flatter and flatter.

4. Discussion and conclusions

To study the mixing of a N_2O-like passive tracer in lower stratospheric surf zones, we proposed a concept model with a "mean gradient" forcing based on the fact that a weak zonal-mean tracer gradient is steadily maintained inside midlatitudes, with the tropics and polar regions acting as a source reservoir and sink, respectively. Within this mean gradient model, tracers fluctuations due to chaotic mixing by planetary-wave breaking can be regarded as being generated from the background mean gradient.

Based on the mean-gradient model, we have taken two theoretical approaches to physically interpret the PDFs of tracer fluctuations. In the Lagrangian formalism, the tracer PDF is obtained from the PDF of Lyapunov exponents. We emphasize that the exponential tails of large tracer fluctuations are not primarily caused by motions unusually persistently against the mean gradient. Instead, these large tracer fluctuations arise from small Lyapunov exponents with which the relevant tracer parcels experience anomalously slow stretching and slow diffusive dissipation. This is because the concentration values of large tracer fluctuations are determined by their "life times" which are associated with small Lyapunov exponents and have exponential distribution. By contrast, large fluctuations due to unusually persistently motions against the mean gradient are random events. The key in the Lagrangian formalism is to evaluate the stretching history that tracer parcels experienced along their journey. The stretching history is characterized by the Lyapunov exponents.

In the conditional closure formalism, the general PDF solution is determined by two conditional quantities: the conditional velocity and dissipation. The conditional velocity characterizes tracer forcing, that is, how tracer fluctuations are generated from the mean background gradient by motions against the mean gradient. As long as the mean gradient is maintained, the conditional velocity remains a linear function of tracer fluctuations. The conditional dissipation characterizes the relationship between the dissipation field (tracer gradients) and tracer fluctuations. For the forced tracer, the conditional dissipation is a time-invariant linear function of the absolute values of tracer fluctuations. The linear properties of the two conditional quantities yield a unique PDF, with a Gaussian core and exponential tails. As discussed in section 2.2, the statistical properties of conditional dissipation and velocity are largely empirical. So far, there is no appropriate theory for interpreting these statistical properties. Pierrehumbert (2000) touched this issue and provided some speculation on conditional dissipation, but did not give an exact answer of how $\langle D \rangle_\theta$ depends on θ. It appears that the properties of these conditional quantities require further studies.

The two classes of approaches provide us with different views on the advection-diffusion problem for a forced passive tracer. The first approach focuses on mixing processes (advection and diffusion) of tracer parcels along their Lagrangian trajectories. It presents us with an unambiguous physical picture and interpretation of how and why large tracer fluctuations display exponential distributions. The second approach directly deals with a well mixed tracer field at the steady state and pursues statistical relationship of conditional forcing and dissipation with tracer fluctuations, while paying little attention to the mixing history of individual tracer parcels. The two approaches seem to complement each other.

The theoretical predictions are first tested with a forced tracer driven by an idealized random flow on a

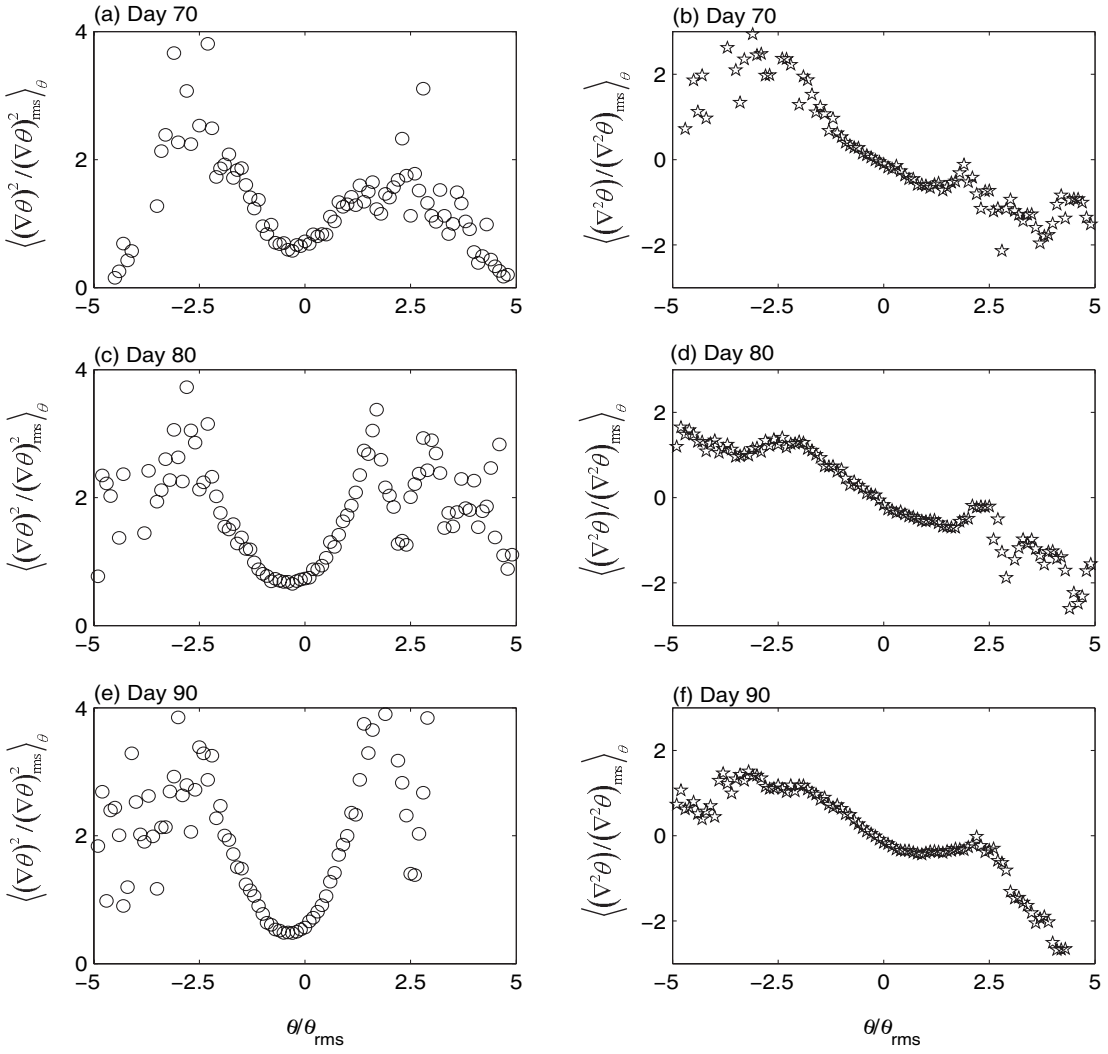

Fig. 10. Conditional dissipation and conditional diffusion for the decaying tracer. The plots on the left side are for conditional dissipation, and the plots on the right side are for conditional diffusion.

sphere. In the mixing zone, a zonal-mean tracer gradient is maintained by forcing, i.e., tracer filaments stretched out from both poles. The results show that conditional velocity is a linear function of tracer fluctuations, and that the conditional dissipation is a positive-definite linear function of tracer fluctuations. There is little evidence showing a parabolic relation for conditional dissipation. The PDFs of tracer fluctuations exhibit a Gaussian core and exponential tails.

Our main interest is whether the theoretical predictions arising from highly idealized flows are applicable to understanding tracer mixing in the stratospheric midlatitudes. The simulation results using ECMWF winds are not completely consistent with the theoretical predictions due to realistic complexity. In the Southern Hemisphere, the conditional dissipation demonstrates a time-invariant, positive-definite linear relation with tracer fluctuations, the conditional velocity is a linear function of tracer fluctuations, and the PDFs exhibit exponential tails. These are fairly consistent with theoretical expectations. In the Northern Hemisphere, the conditional dissipation and velocity also demonstrate linear relations with tracer fluctuations. However, they are much weaker than that in the Southern Hemisphere. The PDFs show short exponential tails bounded by deep and sharp-cut skirts. The deviation of the Northern-Hemisphere PDFs from theoretical expectation is presumably because of too slowly varying strains due to relatively weak wave activity in the Northern Hemisphere in these months. This suggests a limitation of the theories when applied to realistic flows.

We have further more compared the long-term behavior of the PDFs between the forcing and decaying

cases. The difference between the two cases is that the PDF tails of the decaying tracer vary with time and become flatter than exponential after two months, while the PDF tails of the forced tracer remain exponential. Since the linear property of both the conditional velocity in the forcing case and the conditional diffusion in the decaying case is time-invariant, the difference in the PDFs lies in the differences in conditional dissipation. For the forced tracer, the conditional dissipation remains linear when the steady state is reached. By contrast, for the decaying tracer the conditional dissipation evolves from linear to parabolic after two months. It is the time-dependent conditional dissipation in the decaying case that leads to the change in the PDF tails from exponential to algebraic.

Acknowledgements. This work is supported by the National Natural Science Foundation of China (NSFC) under Grants Nos. 40575031 and 40533016, and by the Ministry of Education of China under Grant 106002. I am grateful to the two anonymous reviewers for their constructive comments, which are very helpful for improving this paper.

REFERENCES

Allen, D. R., and Coauthors, 1999: Observations of middle atmosphere CO from the UARS ISAMS during the early northern winter 1991/1992. *J. Atmos. Sci.*, **56**, 563–583.

Balkovsky, E., and A. Fouxon, 1999: Universal long-time properties of Lagrangian statistics in Batchelor regime and their application to passive scalar problem. *Phys. Rev. E*, **60**, 4164–4174.

Castaing, B., and Coauthors, 1989: Scaling of hard thermal turbulence in Rayleigh-Benard convection. *Journal of Fluid Mechanics*, **204**, 1–30.

Chertkov, M., G. Falkovich, I. Kolokolov, and I. Lebedev, 1995: Statistics of a passive scalar advected by a large-scale two-dimensional velocity field: analytic solution. *Phys. Rev. E*, **51**, 5609–5627.

Ching, E. S. C., 1996: General formula for stationary or statistically homogeneous probability density functions. *Phys. Rev. E*, **53**, 5899–5903.

Ching E. S. C., and R. H. Kraichnan, 1998: Exact results for conditional means of a passive scalar in certain statistically homogeneous flows. *Journal of Statistical Physics*, **93**, 787–795.

Edouard, S., B. Legras, F. Lefevre, and R. Eymard, 1996: The effect of small-scale inhomogeneities on ozone depletion in the Arctic. *Nature*, **384**, 444–447.

Eswaran, V., and S. B. Pope, 1988: Direct numerical simulations of the turbulent mixing of a passive scalar. *Physics of Fluids A*, **31**(3), 506–520.

Gollub J. P., J. Clarke, M. Gharib, B. Lane, and O. N. Mesquite, 1991: Fluctuations and transport in a stirred fluid with a mean gradient. *Phys. Rev. Lett.*, **67**, 3507–3510.

Haynes, P., and E. Shuckburgh, 2000: Effective Diffusivity as a diagnostic of atmospheric transport, Part I: stratosphere. *J. Geophys. Res.*, **105**, 2,2777–2,2794.

Holzer, M., and E. D. Siggia, 1994: Turbulent mixing of a passive scalar. *Physics of Fluids*, **6**, 1820–1837.

Hu, Y., and R. T. Pierrehumbert, 2001: The advection-diffusion problem for stratospheric flow, Part I: Concentration probability distribution function. *J. Atmos. Sci.*, **58**, 1493–1510.

Hu, Y., and R. T. Pierrehumbert, 2002: The advection-diffusion problem for stratospheric flow, Part II: Probability distribution function of tracer gradients. *J. Atmos. Sci.*, **59**, 2830–2845.

Jayesh, and Z. Warhaft, 1992: Probability distribution, conditional dissipation, and transport of passive temperature fluctuations in grid-generated turbulence. *Phys. Fluids A*, **4**, 2292–2307.

Kadanoff, L. P., 2000: *Statistical Physics: Statics, Dynamics, and Renormalization*. World Scientific, New Jersey, 483pp.

Lane, B. R., O. N. Mesquita, S. R. Meyers, and J. P. Gollub, 1993: Probability distributions and thermal transport in a turbulent grid flow. *Physics of Fluids A*, **5**, 2225–2263.

Nakamura, N., 1996: Two-dimensional mixing, edge formation, and permeability diagnosed in an area coordinate. *J. Atmos. Sci.*, **53**, 1524–1537.

Nakamura, N., 1998: Leaky containment vessels of air: a Langrangian-mean approach to the stratospheric tracer transport. In *Advances in Fluid Mechanics: Dynamics of Atmospheric Flows. Part I. Atmospheric Transport and Diffusion Processes*, M. P. Singh and S. Raman, Eds., Ashurst Lodge, Comput. Mech. Publ., 193–246.

Nakamura, N., J. Ma, and J. Modi, 1999: Deciphering Lagrangian-mean transport and chemistry from the stratospheric tracer constituents data. In *Recent Advances in Stratospheric Processes*, Nathan and Cordero, Eds. Research Sgnpost India.

Majda, A. J., 1993: The random uniform shear layer: An explicit example of turbulent diffusion with broad tail probability distributions. *Physics of Fluids A*, **5**, 1963–1970.

Majda, A. J., and P. R. Kramer, 1999: Simplified models for turbulent diffusion: Theory, numerical modelling, and physical phenomena. *Physics Report*, **314**, 237–574.

Pierrehumbert, R. T., 2000: Lattice models of Advection-Diffusion. *Chaos*, **10**, 61 –74.

Pierrehumbert, R. T., and H. Yang, 1993: Global chaotic mixing on isentropic surface. *J. Atmos. Sci.*, **50**, 2462–2480.

Pope, S. B., 2000: *Turbulent Flows*. Cambridge University Press, Cambridge, UK, 771pp.

Pumir, A., 1994: A numerical study of the mixing of a passive scalar in three dimensions in the presence of a mean gradient. *Physics of Fluids*, **6**(6), 2118–2132.

Shraiman, B. I., and E. D. Siggia, 1994: Lagrangian path

integrals and fluctuations in random flows. *Phys. Rev. E*, **49**, 2912–2927.

Shraiman, B., and E. D. Siggia, 2000: Scalar turbulence. *Nature*, **405**, 639–646.

Sinai, Ya. G., and V. Yakhot, 1989: Limiting probability distributions of a passive scalar in a random velocity field. *Phys. Rev. Lett.*, **63**, 1962–1964.

Sreenivasan, K. R., and R. A. Antonia, 1997: The phenomenology of small-scale turbulence. *Annual Review of Fluid Mechanics*, **29**, 435–472.

Tan, D. G. H., P. H. Haynes, A. R. MacKenzie, and J. A. Pyle, 1998: The effects of fluid-dynamical stirring and mixing on the deactivation of stratospheric chlorine. *J. Geophys. Res.*, **103**(D1), 1585–1605.

Warhaft, Z., 2000: Passive scalars in turbulent flows. *Annual Review of Fluid Mechanics*, **32**, 203–240.

Yakhot, V., S. A. Orszag, S. Balachandar, E. Jackson, Z. She, and L. Sirovich, 1990: Phenomenological theory of probability distributions in turbulence. *J. Sci. Comput.*, **5**, 199–221.